IEEE Access
Multidisciplinary : Rapid Review : Open Access Journal

Received December 2, 2021, accepted January 16, 2022, date of publication January 27, 2022, date of current version February 7, 2022.

Digital Object Identifier 10.1109/ACCESS.2022.3147412

Robust Estimators for Faster-Than-Nyquist Signaling

ZOUHIR BAHRI, (Member, IEEE)
Department of Electrical and Electronics Engineering, University of Bahrain, Isa Town, Bahrain
e-mail: zkbahri@uob.edu.bh

ABSTRACT Novel, robust, and computationally attractive non-data-aided (NDA) and data-aided (DA) single and joint parameter estimators for faster-than-Nyquist (FTN) signaling are presented. By using the sixth moment alongside the second and fourth, it is possible to formulate an estimator allowing the joint blind estimation of the FTN symbol-packing ratio (SPR) (speed-up parameter) as well as the signal-to-noise ratio (SNR). The proposed estimators are robust in that they are based on uniformly spaced samples of the FTN signal taken at a fairly arbitrary FTN rate, insensitive to carrier and timing phase errors. While avoided in Nyquist signaling, the inter-symbol interference (ISI) term deliberately introduced in FTN signals is advantageously utilized for the estimation of SNR and SPR. The derivations are performed on a general complex base-signaling pulse and are illustrated for the commonly used root-raised cosine (RRC). Novel FTN Cramer-Rao lower bounds (CRLB) are derived to benchmark the efficiency of the proposed estimators. Extensive simulations are provided to illustrate the performance of the proposed estimators with respect to variations in all the relevant parameters and indicate that the estimators work best for the practical range of lower-intermediate values of SPR and SNR. The computational features of the proposed estimators, in addition to their robustness against carrier and sampling errors, make them valuable in many practical applications that incorporate cognitive radio (CR) alongside FTN.

INDEX TERMS Cramer-Rao lower bound (CRLB), faster-than-Nyquist (FTN), parameter estimation, root-raised cosine (RRC), statistical moments, signal-to-noise ratio (SNR), symbol-packing ratio (SPR).

I. INTRODUCTION

Originated by Mazo in 1975 [1], faster-than-Nyquist (FTN) signaling [2 and references therein] has received much attention, driven by a constantly increasing need for faster communications and a more efficient bandwidth utilization. FTN has enjoyed a widespread use in diverse applications such as terabit super-channel transmission [3], [4], satellite communications [5], [6], digital video broadcasting [7], optical communications [8], [9], wireless smart grid security [10], long haul underwater links [11], ultra-high-definition TV [12], and mobile communications [13], [14].

The practical implementation of FTN systems requires the knowledge (or estimate) of some key parameters of the FTN signal, namely the signal-to-noise ratio (SNR) and the symbol packing ratio (SPR). Such parameters are important in many aspects, such as turbo equalization, adaptive coding, and modulation [15]. They are also important in applications that incorporate cognitive radio (CR) alongside FTN, as in 5G mobile communication [16], where an accurate estimate of SNR and SPR is needed for an accurate radio scene analysis, leading to more efficient resource utilization.

Much work has been proposed to estimate SNR for the additive white Gaussian noise (AWGN) channel [17 and references therein]. This includes the so called ''M2M4'' [18] that is based on the second and fourth-order moments of the received signal in addition to an approach [19] that uses up to the sixth-order moment to cater for non-constant modulus constellations. However, all these methods assume AWGN and neglect the effect of the Inter-Symbol Interference (ISI) by assuming Nyquist timing with no sampling errors. Such assumptions are obviously invalid with FTN signals that are characterized by a large ISI, in addition to *colored* noise. The open literature contains almost no work related to estimating the SNR of FTN signals, except for a recent report by Liang *et al.* [20], which used a code-aided approach based on expectation maximization (EM). Their proposed iterative algorithm requires a noise decorrelation by applying

The associate editor coordinating the review of this manuscript and approving it for publication was Jian Song.

the Cholesky factorization to the covariance matrix of the colored noise following the receiver's matched filter. The simulation results show that the mean squared error (MSE) of the estimated SNR asymptotically approaches the standard Nyquist timing data-aided (DA) Cramer Rao lower bound (CRLB) [21] for higher values of SNR. However, this method has several limitations. First, it assumes perfect timing with no sampling phase errors. Second, it is computationally expensive because of the Cholesky factorization, in addition to its iterative nature with a convergence that depends on the initial estimate. Third, it exhibits a "waterfall" threshold effect wherein the MSE sharply increases for SNR lower than approximately 3 dB on average.

In parallel, much attention has also been given to estimating the data symbol rate for Nyquist signaling, mostly focusing on utilizing the cyclostationarity of the signal's statistical moments [22], with little emphasis given to the estimation of the SPR of FTN signals. The most noticeable recent report in this context is the work by Song *et al.* [23], which uses a deep-learning approach for SPR estimation. This method searches for the most likely SPR over a discrete grid of possible values using a 5-layer deep neural network (DNN). In addition to its resolution issue and high computational cost, this method requires retraining of its DNN whenever there are changes in the system parameters; hence, it is less flexible to adapt to changing scenarios. In the only other report related to the estimation of the symbol rate of FTN signals [24], Abello *et al.* showed that these are not second-order cyclostationary. Hence, the second-order moment usually used for Nyquist signaling is insufficient to estimate the data symbol rate for FTN, requiring the use of the fourth-order moment. Exploiting the fact that the latter exhibits peaks in its spectral signature, a heuristic method was presented to search for the maximum value in the spectral moment function. However, no conclusive results have been obtained regarding the efficiency of this method.

To the author's knowledge, no work can be found in the open literature about a *joint blind* estimation of the SNR and SPR of FTN signals. In this paper, we address this gap by proposing novel robust estimators that use the sixth moment alongside the fourth and second. They are computationally efficient because they are based on simple time-averages that may be enhanced online as more samples are gathered. The proposed estimators are also robust in the sense that they are insensitive to carrier and timing errors, requiring only uniform samples of the received signal (following the matched filter) taken at a fairly arbitrary FTN rate with an arbitrary sampling phase. Finally, this work also fills another gap in the open literature related to the absence of CRLB in the context of FTN signaling for both SNR and SPR.

The remainder of this paper is organized as follows. Section 2 is used to formulate the problem and establish the notations used. In Section 3, we present some fundamental results related to the statistical moments of the FTN signal. Section 4 is devoted to the derivation of the proposed DA and blind (NDA) joint and single estimators for the two main FTN parameters, SNR and SPR. In Section 5, we derive novel FTN CRLBs to benchmark the efficiency of the proposed estimators. Section 6 is used to present the simulation results for the special case of the root-raised cosine (RRC) signaling pulse. Finally, Section 7 summarizes and concludes the paper.

II. PROBLEM FORMULATION AND NOTATION SETUP

In this work, we focus on estimating the SNR and SPR of the base-band signal of a single channel in a multitone FTN signal following carrier demodulation. The present treatment is in the context of a flat channel, wherein the ISI is not due to channel dispersions, but to the non-orthogonal signaling coupled with sampling errors. The case of dispersive channels may be generalized, but at the expense of simplicity and clarity of the following analysis. We assume a general case of complex, unit-energy signaling pulse $p(t)$ with an autocorrelation denoted by $\hat{p}(t)$. The latter is assumed to be orthogonal with respect to T, the time interval between two adjacent ISI-free symbols, that is, the inverse of the Nyquist rate.

In the following, we assume that $p(t)$ is band-limited to $1/T$, hence $P(f) = 0$ for $|f| \geq 1/T$, with $P(f)$ denoting the Fourier transform of $p(t)$. Consequently, the k^{th}-order real-valued auto-convolution of $|P(f)|^2$, denoted by $\hat{P}_k(f)$ for $k = 0, 1, \ldots$ (with $\hat{P}_0(f) \equiv |P(f)|^2$), vanishes out of the interval [-$(k+1)/T$, $(k+1)/T$]. Hence, the autocorrelation of $p(t)$ (real and even-symmetric) is given by:

$$\hat{p}(t) = \int_{-1/T}^{1/T} |P(f)|^2 e^{j2\pi ft} df = \int_{-1/T}^{1/T} \hat{P}_0(f) e^{j2\pi ft} df. \quad (1)$$

Using the convolution property of the Fourier transform, $\hat{P}_{k-1}(f)$ is related to the k^{th} power of $\hat{p}(t)$ as:

$$\hat{p}^k(t) = \int_{-k/T}^{k/T} \hat{P}_{k-1}(f) e^{j2\pi ft} df; \quad k = 1, 2, \ldots \quad (2)$$

and may be expressed in terms of the following recursion

$$\begin{aligned}\hat{P}_k(f) &= \int_{-k/T}^{k/T} \hat{P}_{k-1}(u) \hat{P}_0(f-u) du \\ &= \int_{-(k-p)/T}^{(k-p)/T} \hat{P}_{k-p}(u) \hat{P}_{p-1}(f-u) du; \\ & \quad p = 1, \ldots [k/2] \end{aligned} \quad (3)$$

where $[k/2]$ denotes the largest integer closest to $k/2$. Using (3), we note the following special case of $\hat{P}_{2k+1}(f)$ $(k = 0, 1, 2, \ldots)$ (odd-ordered auto-convolution of $\hat{P}_0(f)$):

$$\hat{P}_{2k+1}(f) = \int_{-(k+1)/T}^{(k+1)/T} \hat{P}_k(u) \hat{P}_k(f-u) du; \quad (4)$$

hence,

$$\hat{P}_{2k+1}(0) = \int_{-(k+1)/T}^{(k+1)/T} \left[\hat{P}_k(u)\right]^2 du = 2\int_{0}^{(k+1)/T} \left[\hat{P}_k(u)\right]^2 du \tag{5}$$

owing to the even symmetry of $\hat{P}_k(u)$.

We assume that the pulses $p(t)$ are modulated by M-ary circularly symmetric[1] complex data symbols (e.g., MPSK and MQAM, $M \geq 4$) denoted by d_n, and are transmitted at the FTN rate, that is, at multiples of $\hat{T} = \alpha T$ where $\alpha(\leq 1)$ is the SPR. We assume d_n to be zero-mean, independent, and uniformly distributed, satisfying the following conditions:

$$\mathbb{E}\{d_n\} = 0 = \mathbb{E}\{d_n d_m\}; \quad \textit{for all } n, m \tag{6}$$

and

$$\mathbb{E}\left\{d_n d_m^*\right\} = \delta_{nm} \tag{7}$$

where "$*$" denotes the complex conjugate, $\mathbb{E}\{.\}$ the expected value, and $\delta_{n,m}$ is the Kronecker delta function (equal to 1 for $n = m$ and zero otherwise). The independence of the data symbols as well as (6) and (7) straightforwardly lead to the following useful generalizations:

$$\mathbb{E}\left\{\prod_{i=1}^{N} d_{n_i}\right\} = 0 \quad \forall N, n_i \tag{8}$$

and

$$\mathbb{E}\left\{\left[\prod_{i=1}^{N} d_{n_i}\right]\left[\prod_{j=1}^{M} d_{m_j}^*\right]\right\} = 0; \quad \textit{if } N \neq M \textit{ and } \forall n_i, m_j \tag{9}$$

and

$$\mathbb{E}\left\{\left[\prod_{i=1}^{K} d_{n_i}\right]\left[\prod_{j=1}^{K} d_{m_j}^*\right]\right\} = \begin{cases} \psi_q & \textit{if } \{n_i\} \,\bar{\bar{2}}_{K_q}\, \{m_j\}, q = 1, \ldots, K \\ 0 & \textit{otherwise} \end{cases} \tag{10}$$

where ψ_q accounts for non-constant-energy symbol constellations ($\psi_q = 1$ for M-PSK), and $\bar{\bar{2}}_{K_q}$ denotes the q^{th} pairwise-equal combination between $\{n_i; i \in \mathbb{N}_K\}$ and $\{m_j; j \in \mathbb{N}_K\}$ with $\mathbb{N}_K$ denoting set $\{1, \ldots K\}$, $K \geq 2$. For example, such combinations include the case where all indexes are equal, that is, $\{n_1 = m_1 = n_2 = m_2 = \ldots = n_K = m_K\}$, all the cases of a single distinct pair with all other indexes equal, namely $\{(n_k = m_l) \textit{ and } (n_i = n_j = m_i = m_j \neq n_k); \textit{ for all } i \neq k \textit{ and } j \neq l\}$, …etc., ending with the case where all K pairs are distinct. The following two special cases corresponding to $K = 2$ and $K = 3$ illustrate the result in (10) and are used in subsequent sections:

$$\begin{aligned}\mathbb{E}&\left\{d_{n_1} d_{n_2} d_{m_1}^* d_{m_2}^*\right\} \\ &= \eta_4 \delta_{n_1 n_2}\delta_{n_1 m_1}\delta_{n_1 m_2} + \delta_{n_1 m_1}\delta_{n_2 m_2}(1 - \delta_{n_1 n_2}) \\ &\quad + \delta_{n_1 m_2}\delta_{n_2 m_1}(1 - \delta_{n_1 n_2}) \\ &= (\eta_4 - 2)\delta_{n_1 n_2}\delta_{n_1 m_1}\delta_{n_1 m_2} + \delta_{n_1 m_1}\delta_{n_2 m_2} + \delta_{n_1 m_2}\delta_{n_2 m_1}\end{aligned} \tag{11}$$

and

$$\begin{aligned}\mathbb{E}&\left\{d_{n_1} d_{n_2} d_{n_3} d_{m_1}^* d_{m_2}^* d_{m_3}^*\right\} \\ &= \eta_6\left(\delta_{n_1 n_2}\delta_{n_1 n_3}\delta_{n_1 m_1}\delta_{n_1 m_2}\delta_{n_1 m_3}\right) \\ &\quad + \eta_4 \sum_{u=1}^{3}\sum_{v=1}^{3} \delta_{n_u m_v}\left[\delta_{n_i m_k}\delta_{n_j m_l}\delta_{n_i n_j}(1 - \delta_{n_u n_i})\right] \\ &\quad + \sum_{q=1}^{3} \delta_{n_1 m_q}\left[\left(\delta_{n_2 m_a}\delta_{n_3 m_b} + \delta_{n_2 m_b}\delta_{n_3 m_a}\right)\right. \\ &\quad \left.\times\left(1 - \delta_{n_2 n_3}\right)\left(1 - \delta_{n_1 n_2}\right)\left(1 - \delta_{n_1 n_3}\right)\right] \\ &= (\eta_6 - 9\eta_4 + 12)\left(\delta_{n_1 n_2}\delta_{n_1 n_3}\delta_{n_1 m_1}\delta_{n_1 m_2}\delta_{n_1 m_3}\right) \\ &\quad + (\eta_4 - 2)\sum_{u=1}^{3}\sum_{v=1}^{3} \delta_{n_u m_v}\left[\delta_{n_i m_k}\delta_{n_j m_l}\delta_{n_i n_j}\right] \\ &\quad + \sum_{q=1}^{3} \delta_{n_1 m_q}\left[\left(\delta_{n_2 m_a}\delta_{n_3 m_b} + \delta_{n_2 m_b}\delta_{n_3 m_b}\right)\right]\end{aligned} \tag{12}$$

where in the above, $i \neq j \in \mathbb{N}_3 \backslash \{u\}$, $k \neq l \in \mathbb{N}_3 \backslash \{v\}$, $a \neq b \in \mathbb{N}_3 \backslash \{q\}$, and η_4 and η_6 denote the expected value of the fourth and sixth powers of the modulus of d_n, respectively.

$$\mathbb{E}\left\{|d_n|^4\right\} = \eta_4 \tag{13}$$

and

$$\mathbb{E}\left\{|d_n|^6\right\} = \eta_6. \tag{14}$$

For M-PSK $\eta_4 = \eta_6 = 1$, however, for M-QAM, this is not the case. For example, for a square 64-QAM data constellation, the equally likely symbols (given by $d_n = a_n + jb_n$ where $a_n, b_n \in \{\pm V, \pm 3V, \ldots\}$ with $V = 1/\sqrt{42}$) have $\eta_4 = 609/441$ and $\eta_6 = 20613/9261$. Similarly for 16-QAM, $V = 1/\sqrt{10}$ with $\eta_4 = 33/25$ and $\eta_6 = 49/25$.

Next, let $w(t)$ denote the complex, circularly symmetric, wide-sense stationary (WSS), and zero-mean AWGN with a two-sided power spectral density (PSD) equal to $N_0/2$ (real and imaginary part each has a PSD of $N_0/4$). We assume that $w(t)$ is added to the transmitted FTN signal, resulting in the following complex baseband signal in one receiver channel after carrier demodulation:

$$r(t) = \left[e^{j\phi(t)}\right]\sqrt{E_s}\sum_{m=-\infty}^{\infty} d_n p\left(t - m\hat{T}\right) + w(t) \tag{15}$$

[1]For the sake of clarity and conciseness, we opted to focus on the more commonly treated circular signaling (e.g., MPSK and MQAM, M $\geq$ 4) corrupted by circularly symmetric Gaussian noise. The case of non-circular signaling corrupted by non-circular noise may be treated in a similar manner, except that it involves extended statistics with a more elaborate combinatorial. For example, the fourth-order moment of a zero-mean circular complex Gaussian variable is twice its variance, while for a real Gaussian RV it is three times its variance.

where E_s denotes the symbol energy and $\phi(t)$ accounts for possible carrier phase errors and/or frequency offsets. It is assumed that $\phi(t)$ varies relatively slowly with time, so it may be considered to be constant over the observation interval. We assume that the receiver is based on the symbol-by-symbol approach [25] rather than the trellis-based sequence detector algorithm [26]. Hence, the receiver consists of a filter matched to $p(t)$ followed by a soft interference cancellation equalizer [25]. The output of the matched filter is given by

$$y(t) = \hat{w}(t) + \hat{s}(t) \tag{16}$$

where $\hat{s}(t)$ represents the signal-related part of the output (desired sample plus ISI) and is given by

$$\hat{s}(t) = \left[e^{j\phi}\right]\sqrt{E_s}\sum_{m=-\infty}^{\infty} d_m \hat{p}(t - m\alpha T) \tag{17}$$

where $\phi(t)$ is assumed to be constant over the interval of interest, $\hat{p}(t)$ is given by (1), and w(t) is the noise output of the matched filter that is still zero-mean Gaussian, but *colored* noise. Its PSD is given by

$$S_{\hat{w}}(f) = \frac{N_0}{2}|P(f)|^2, \tag{18}$$

with a correlation function given by

$$\begin{aligned} R_{\hat{w}}(\tau) \equiv \mathbb{E}\left\{\hat{w}(t)\hat{w}^*(t+\tau)\right\} &= \frac{N_0}{2}\int_{-\infty}^{\infty}|P(f)|^2 e^{j2\pi f\tau}df \\ &= \frac{N_0}{2}\hat{p}(\tau), \end{aligned} \tag{19}$$

and variance equal to

$$\sigma_{\hat{w}}^2 = \frac{N_o}{2}, \tag{20}$$

because $\hat{p}(0) = 1$, a direct consequence of the unit-energy assumption of $p(t)$. We further assume that $y(t)$ in (16) is sampled at $t = (n+\beta)\varepsilon\alpha T$ (for a total of K samples), where β and ε respectively, account for the sampling phase and rate errors with $|\beta| \leq 0.5$, and while ε is allowed to be an arbitrary real number, it is practically expected to be close to unity. Hence, the n^{th} sample of the matched filter output, denoted by $y[n]$ is given by:

$$\begin{aligned} y[n] &\equiv y((n+\beta)\varepsilon\alpha T) \\ &= \hat{s}[n] + \hat{w}[n] \quad \text{for } n = 0, \ldots, K-1, \end{aligned} \tag{21}$$

where

$$\hat{w}[n] \equiv \hat{w}((n+\beta)\varepsilon\alpha T) \tag{22}$$

and

$$\hat{s}[n] \equiv \left[e^{j\phi}\right]\sqrt{E_s}\sum_{m=-\infty}^{\infty} d_m\hat{p}([(n+\beta)\varepsilon - m]\alpha T). \tag{23}$$

As a prelude to the forthcoming results on the statistics of the FTN signal as well as the estimator derivations, we present the following pivotal proposition related to the power series of the base pulse $\hat{p}(t)$.

Proposition 1: Let $\mathcal{S}_k$ denote the power series of $\hat{p}([\lambda - n]\alpha T)$ where λ is an arbitrary real number independent of n. Then, $\mathcal{S}_k$ is finite, *independent of* λ for the *sufficient* condition[2] $0 < \alpha \leq 1/k$, inversely proportional to αT and is compactly given by

$$\begin{aligned} \mathcal{S}_k &= \sum_{n=-\infty}^{\infty}\left[\hat{p}([n-\lambda]\alpha T)\right]^k \\ &= \frac{\mu_{k-1}}{\alpha}; \quad k = 1, 2\ldots; \ \textit{for } 0 < \alpha \leq 1/k. \end{aligned} \tag{24}$$

where μ_{k-1} is independent of α and λ and is given by

$$\mu_k \equiv \frac{\hat{P}_k(0)}{T}; \quad k = 0, 1, \ldots \tag{25}$$

Proof of Proposition 1: The proof follows from the substitution of $\hat{p}^k(.)$ of (2) into the right-hand side (RHS) of (24), interchanging the order of the summation and integration, and using the standard result

$$\begin{aligned} \sum_{n=-\infty}^{\infty} e^{\pm j2\pi nau} &= \delta(au) \\ &= \frac{1}{|a|}\delta(u); \quad \textit{for } |au| < 1, \end{aligned} \tag{26}$$

where $\delta(u)$ is the Dirac delta function. This completes the proof of Proposition 1. The fact that $\mathcal{S}_k$ in (24) is independent of λ is remarkable and is the reason behind the robustness of the estimators against sampling frequency and phase errors.

III. ON THE STATISTICAL MOMENTS OF THE FTN SIGNAL

This section sheds light on the statistical moments of the FTN signal that will be used for the derivation of the upcoming estimators. The following propositions first focus on the FTN's *colored* noise $\hat{w}[n]$, then on its signal-related part $\hat{s}[n]$.

Proposition 2:

$$\begin{aligned} &\mathbb{E}\left\{\left(\hat{w}[n_1]\right)^{a_1}\left(\hat{w}^*[n_2]\right)^{a_2}\right\} \\ &\quad = \delta_{a_1a_2}[a_1!]\left[\frac{N_0}{2}\hat{p}(|n_1 - n_2|\varepsilon\alpha T)\right]^{a_1} \end{aligned} \tag{27}$$

Proof of Proposition 2: Using the standard result on the expected value of the product of zero-mean Gaussian random variables [27] (being the sum of the products of the expected value of all pair-wise combinatorial of these random variables), in addition to the circularity [28] assumption of $w(t)$ (leading to the fact that $\mathbb{E}\left\{\left(\hat{w}[n]\right)^a\right\} = 0; \forall a, n$), as well as (19) and (22) we get the result of (27), where "$a_1!$" denotes the factorial of a_1 (equal to the total number of combinations that distinctly pair each of the "a_1" $\hat{w}[n_1]$ terms with one of the "a_1" $\hat{w}^*[n_2]$ terms). This completes the proof of Proposition 2.

[2]Practically the range $0 < \alpha \leq 1/k$ may be relaxed in case the support of $H(f)$ is less than $1/T$. For example, for RRC, $H(f)$ is zero for $f > (1+r)/2T$, hence, the *sufficient* condition on α becomes $0 < \alpha \leq 2/[k(1+r)]$. As illustrated in the computer simulations of Section 6, it turns out that the range of α may practically be expanded even further.

Proposition 3: The even-ordered moments of $\hat{w}[n]$, denoted by $\mathcal{M}_{\hat{w}_{2q}}$ $(q = 1, 2, \ldots)$, are given by

$$\mathcal{M}_{\hat{w}_{2q}} = \mathbb{E}\left\{\left|\hat{w}[n]\right|^{2q}\right\} = [q!]\,[N_0/2]^q \tag{28}$$

Proof of Proposition 3: Using the fact that $\hat{p}(0) = 1$, (28) is a special case of (27) with $n_1 = n_2$ and $a_1 = a_2 = q$. This completes the proof of Proposition 3.

Proposition 4: Let $\mathcal{M}_{\hat{s}_{2q}}(q = 1, 2, 3)$ denote the first three even-ordered moments of $\hat{s}[n]$ in (23), defined by

$$\mathcal{M}_{\hat{s}_{2q}} = \mathbb{E}\left\{\left|\hat{s}\,[n]\right|^{2q}\right\}; \quad q = 1, 2, 3 \tag{29}$$

Then, $\mathcal{M}_{\hat{s}_{2q}}(q = 1, 2, 3)$ is irrespective of ϕ, β, n, ε, and is given by the sum of products of powers of $\mathcal{S}_{2q}$ $(q = 1, 2, 3)$ that only depend on α, $\hat{P}_{k-1}(0)$, and T. Namely, we have

$$\mathcal{M}_{\hat{s}_2} = E_s\mathcal{S}_2 \tag{30}$$

and

$$\mathcal{M}_{\hat{s}_4} = E_s^2\left[(-2+\eta_4)\mathcal{S}_4 + 2\left(\mathcal{S}_2\right)^2\right] \tag{31}$$

and

$$\mathcal{M}_{\hat{s}_6} = E_s^3\left[(\eta_6 - 9\eta_4 + 12)\mathcal{S}_6 + 9(-2+\eta_4)\mathcal{S}_2\mathcal{S}_4 + 6\left(\mathcal{S}_2\right)^3\right] \tag{32}$$

Proof of Proposition 4: First, the independence of $\mathcal{M}_{\hat{s}_{2q}}$ from the carrier phase term ϕ is a direct consequence of using the modulus of $\hat{s}\,[n]$. Second, the results of (30)-(32) follow by applying (23) to (29) and simplifying the summations using the earlier results of (8)-(14) alongside (24). This completes the proof of Proposition 4.

Proposition 5: Let $\mathcal{M}_{y_{2q}}$ $(q = 1, 2, 3)$ denote the first three even-ordered moments of the FTN signal $y[n]$ in (21), defined by

$$\mathcal{M}_{y_{2q}} = \mathbb{E}\left\{\left|y\,[n]\right|^{2q}\right\}; \quad q = 1, 2, 3, \tag{33}$$

then $\mathcal{M}_{y_{2q}}$ $(q = 1, 2, 3)$ is explicitly given by

$$\mathcal{M}_{y_2} = \mathcal{M}_{\hat{s}_2} + \mathcal{M}_{\hat{w}_2} = \frac{\mu_1 E_s}{\alpha} + N_o/2 \tag{34}$$

$$\begin{aligned}\mathcal{M}_{y_4} &= \mathcal{M}_{\hat{s}_4} + 4\mathcal{M}_{\hat{s}_2}\mathcal{M}_{\hat{w}_2} + \mathcal{M}_{\hat{w}_4}\\ &= -\frac{\hat{\mu}_3 E_s^2}{\alpha} + 2\mathcal{M}_{y_2}^2\end{aligned} \tag{35}$$

$$\begin{aligned}\mathcal{M}_{y_6} &= \mathcal{M}_{\hat{s}_6} + 9\mathcal{M}_{\hat{s}_4}\mathcal{M}_{\hat{w}_2} + 9\mathcal{M}_{\hat{s}_2}\mathcal{M}_{\hat{w}_4} + \mathcal{M}_{\hat{w}_6}\\ &= \frac{\hat{\mu}_5 E_s^3}{\alpha} + 9\mathcal{M}_{y_4}\mathcal{M}_{y_2} - 12\mathcal{M}_{y_2}^3\end{aligned} \tag{36}$$

where $\mu_k(k = 0, 1, \ldots)$ is defined by (25) with $\hat{\mu}_3$ and $\hat{\mu}_5$ respectively given by

$$\hat{\mu}_3 = (2 - \eta_4)\,\mu_3 \tag{37}$$

$$\hat{\mu}_5 = (\eta_6 - 9\eta_4 + 12)\,\mu_5 \tag{38}$$

Proof of Proposition 5: The results in (34)-(38) directly follow from applying (21) to (33) and utilizing (8)-(10), (27), (28), and (30)-(32), along with the independence of $\hat{s}\,[n]$and $\hat{w}[n]$. This completes the proof of Proposition 5.

In the following sections, several estimators are proposed with the objective of estimating SPR $(= \alpha)$ as well as SNR $(= E_s/N_o)$ independently of the carrier phase errors and/or slowly varying frequency offsets $(= \phi)$ as well as the timing phase errors $(= \beta)$ and to a practical extent the sampling rate offsets $(= \varepsilon)$.

IV. ESTIMATORS DERIVATIONS

A. JOINT BLIND (NDA) ESTIMATORS

Let $\mathcal{K}_y$ denote the kurtosis of the FTN signal, given by

$$\mathcal{K}_y = \frac{(\mathcal{M}_{y_4} - 2\mathcal{M}_{y_2}^2)}{\mathcal{M}_{y_2}^2}. \tag{39}$$

Then, simple algebraic manipulations of (34)–(36) lead to the following joint and blind (NDA) estimators of E_s $(\equiv E_{s_{JNDA}})$, N_0 $(\equiv N_{0_{JNDA}})$, SNR $(\equiv SNR_{JNDA})$, and SPR $(\equiv \alpha_{JNDA})$.

$$E_{s_{JNDA}} = \frac{\hat{\mu}_3}{4\hat{\mu}_5}\left(\frac{-\mathcal{M}_{y_6} + 9\mathcal{M}_{y_4}\mathcal{M}_{y_2} - 12\mathcal{M}_{y_2}^3}{\mathcal{K}_y\mathcal{M}_{y_2}^2}\right) \tag{40}$$

$$N_{0_{JNDA}} = 2\left(\mathcal{M}_{y_2} - \frac{\mu_1 E_{s_{JNDA}}}{\alpha_{JNDA}}\right) \tag{41}$$

$$SNR_{JNDA} \equiv E_{s_{JNDA}}/N_{0_{JNDA}} \tag{42}$$

$$\alpha_{JNDA} = \frac{-\hat{\mu}_3 E_{s_{JNDA}}^2}{\mathcal{K}_y\mathcal{M}_{y_2}^2} \tag{43}$$

where $\mathcal{K}_y$, μ_1, $\hat{\mu}_3$, and $\hat{\mu}_5$ are provided by (39), (25), (37), and (38), respectively. Note that the division by $\mathcal{K}_y$ in (40), (43), and the following derivations is justified by a recent analytic investigation into the statistical characteristics of the FTN signal [29], formally establishing that it is *always* sub-Gaussian (Platy-kurtotic) with $-2 \leq \mathcal{K}_y < 0$.

B. SINGLE BLIND (NDA) ESTIMATORS

Assuming α to be known, while ε is still allowed to vary in order to cater to possible sampling frequency errors, simple manipulations of (34) and (35) lead to the following blind single estimator of $E_s(\equiv E_{s_{SNDA}})$, N_0 $(\equiv N_{0_{SNDA}})$, and SNR $(\equiv SNR_{SNDA})$.

$$E_{s_{SNDA}} = \sqrt{\frac{\alpha\left(2\left[\mathcal{M}_{y_2}\right]^2 - \mathcal{M}_{y_4}\right)}{\hat{\mu}_3}} \tag{44}$$

$$N_{0_{SNDA}} = 2\left(\mathcal{M}_{y_2} - \frac{\mu_1 E_{s_{SNDA}}}{\alpha}\right) \tag{45}$$

$$SNR_{SNDA} \equiv E_{s_{SNDA}}/N_{0_{SNDA}} \tag{46}$$

On the other hand, assuming SNR $(\equiv E_s/N_0)$ to be known, we obtain from (34) and (35) the following quadratic equation in α:

$$\alpha^2 + 4\alpha\,(SNR)\left(\mu_1 + \frac{\mu_3\,(SNR)}{\mathcal{K}_y}\right) + \left[2\,(SNR)\,\mu_1\right]^2 = 0 \tag{47}$$

that has the following valid solution for the entire range of α and SNR. Thus, we obtain the single blind estimator of SPR

($\equiv \alpha_{SNDA}$) as

$$\alpha_{SNDA} = \frac{-2(SNR)^2\hat{\mu}_3}{\mathcal{K}_y}\left[\frac{\mathcal{K}_y\mu_1}{(SNR)\hat{\mu}_3}+1-\sqrt{1+\frac{2\mathcal{K}_y\mu_1}{(SNR)\,\hat{\mu}_3}}\right] \tag{48}$$

where it can be easily verified that the term under the square root is always positive, namely,

$$1+\frac{2\mathcal{K}_y\mu_1}{(SNR)\hat{\mu}_3} \geq 0 \Leftrightarrow \left[(SNR)\,\mu_1-\frac{\alpha}{2}\right]^2 \geq 0; \tag{49}$$

the right inequality being always true.

C. JOINT DA ESTIMATORS

This section presents a DA joint estimator that uses DA (in addition to NDA[3]) first and second moments only. Even though a DA approach incurs some cost on the density of the FTN signal, this method is appealing owing to its efficiency, as demonstrated by the upcoming simulation section. Here, we assume K transmitted data symbols to be known at the receiver; hence, without loss of generality, we set $d_n = 1$ in (23) without affecting the characteristics of the noise process $\hat{w}[n]$ [21]. Using the result of (24), the DA FTN signal model of (21)-(23) becomes

$$\begin{aligned} y_{DA}[n] &= \hat{w}[n] + e^{j\phi}\sqrt{E_s}\sum_{m=-\infty}^{\infty}\hat{p}\left([(n+\beta)\,\varepsilon-m]\,\alpha T\right) \\ &= \hat{w}[n] + \mathcal{S}_1 e^{j\phi}\sqrt{E_s} = \hat{w}[n] + \frac{\mu_0 e^{j\phi}\sqrt{E_s}}{\alpha}; \\ &\quad for\ n = 0\ldots, K-1. \end{aligned} \tag{50}$$

Referring to (50), the magnitudes of the first and second DA moments of $y_{DA}[n]$, denoted by $|\mathcal{M}_{DAy_1}|$ and $|\mathcal{M}_{DAy_2}|$, are given by

$$|\mathcal{M}_{DAy_1}| = \frac{\mu_0\sqrt{E_s}}{\alpha} \tag{51}$$

$$\begin{aligned} |\mathcal{M}_{DAy_2}| = \mathcal{M}_{DAy_2} &= \frac{\mu_0^2 E_s}{\alpha^2}+\frac{N_o}{2} \\ &= |\mathcal{M}_{DAy_1}|^2+\frac{N_0}{2}. \end{aligned} \tag{52}$$

Using (51) and (52) as well as the second NDA moment of the FTN signal in (34), we obtain the following joint DA estimates of $E_s(\equiv E_{s_{JDA}})$, N_0 ($\equiv N_{0_{JDA}}$), SNR ($\equiv SNR_{JDA}$), and SPR ($\equiv \alpha_{JDA}$):

$$E_{s_{JDA}} = \left[\frac{\mu_0}{|\mathcal{M}_{DAy_1}|\,\mu_1}\left(\mathcal{M}_{y_2}-\mathcal{M}_{DAy_2}+|\mathcal{M}_{DAy_1}|^2\right)\right]^2 \tag{53}$$

$$N_{0_{JDA}} = 2\left(\mathcal{M}_{DAy_2}-|\mathcal{M}_{DAy_1}|^2\right) \tag{54}$$

$$SNR_{JDA} = \frac{E_{s_{JDA}}}{N_{0_{JDA}}} \tag{55}$$

$$\alpha_{JDA} = \frac{\mu_0}{|\mathcal{M}_{DAy_1}|}\sqrt{E_{s_{JDA}}} \tag{56}$$

[3]As such, the estimators may be thought of as hybrid, where it is assumed that an estimate of the NDA second moment is available prior to sending the data preamble and calculating the DA moments.

D. SINGLE DA ESTIMATORS

Assuming α to be known, using (51) and (52), we obtain the following single DA estimates of $E_s(\equiv E_{s_{SDA}})$, N_0 ($\equiv N_{0_{SDA}}$), and SNR ($\equiv SNR_{SDA}$):

$$E_{s_{SDA}} = \left[\frac{\alpha}{\mu_0}|\mathcal{M}_{DAy_1}|\right]^2 \tag{57}$$

$$N_{0_{SDA}} = 2\left(\mathcal{M}_{DAy_2}-|\mathcal{M}_{DAy_1}|^2\right) \tag{58}$$

$$SNR_{SDA} = \frac{E_{s_{SDA}}}{N_{0_{SDA}}} \tag{59}$$

On the other hand, assuming SNR is known, a single DA estimate of SPR($\equiv \alpha_{SDA}$) is obtained from (51) and (52) as

$$\alpha_{SDA} = \frac{\mu_0\sqrt{2SNR\left(\mathcal{M}_{DAy_2}-|\mathcal{M}_{DAy_1}|^2\right)}}{|\mathcal{M}_{DAy_1}|} \tag{60}$$

V. ESTIMATOR BENCHMARKS

In this section, we present novel DA CRLBs for both SNR and SPR, respectively denoted by $CRLB_{FTN\_SNR}$ and $CRLB_{FTN\_\alpha}$ which are used to benchmark the efficiency of the proposed estimators. It is shown that $CRLB_{FTN\_SNR}$ tends in the limiting case of Nyquist signaling (i.e., $\alpha = \varepsilon = 1$; $\beta = 0$) to the standard DA CLRB [21] (denoted by $CRLB_{Nyq\_SNR}$).

Referring to the DA FTN signal in (50), it is more conveniently reformulated in the following K^{th}-dimensional vector space form:

$$\boldsymbol{y}_{DA} = \boldsymbol{\mu} + \hat{\boldsymbol{w}} \tag{61}$$

where $\boldsymbol{y}_{DA} = [y_{DA}[0]\ldots y_{DA}[K-1]]^T$, $\boldsymbol{\mu} = \mu_0\frac{e^{j\phi}\sqrt{E_s}}{\alpha}\boldsymbol{u}$, $\boldsymbol{u} = [1\ldots 1]^T$, $\hat{\boldsymbol{w}} = [\hat{w}[0]\ldots\hat{w}[K-1]]^{\boldsymbol{T}}$, and $[.]^{\boldsymbol{T}}$ denotes the transpose operation. Referring to (61) and (27), the vector y is Gaussian with mean $\boldsymbol{\mu}$ and covariance matrix $\boldsymbol{C}_y$ defined by

$$\boldsymbol{C}_y = \mathbb{E}\left\{(\boldsymbol{y}_{DA}-\boldsymbol{\mu})(\boldsymbol{y}_{DA}-\boldsymbol{\mu})^{*T}\right\} = \boldsymbol{C}_{\hat{w}} \tag{62}$$

where $\boldsymbol{C}_{\hat{w}}$ is the $K\times K$ positive definite symmetric covariance matrix defined by its (i^{th}, j^{th}) entry as:

$$\begin{aligned} \boldsymbol{C}_{\hat{w}_{ij}} &= E\left\{\hat{w}[i]\hat{w}^*[j]\right\} = \frac{N_0}{2}\hat{p}\left(|i-j|\,\varepsilon\alpha T\right); \\ &\quad for\ i,j \in \{0\ldots, K-1\} \end{aligned} \tag{63}$$

To decorrelate the colored noise $\hat{w}[.]$, the Cholesky factorization [20] is applied to the covariance matrix $C_{\hat{w}}$ to yield

$$\boldsymbol{C}_{\hat{w}} = \frac{N_0}{2}\boldsymbol{L}\boldsymbol{L}^T. \tag{64}$$

Next, the following bijective transformation is applied to the data vector $\boldsymbol{y}_{DA}$ (without altering its statistical sufficiency):

$$z = \boldsymbol{L}^{-1}\boldsymbol{y}_{DA} = \frac{\sqrt{E_s}}{\alpha}\boldsymbol{v} + \hat{\hat{\boldsymbol{w}}} \tag{65}$$

with

$$\hat{\hat{\boldsymbol{w}}} = \boldsymbol{L}^{-1}\hat{\boldsymbol{w}} \tag{66}$$

and

$$\boldsymbol{v} = \mu_0 e^{j\phi} \boldsymbol{L}^{-1}\boldsymbol{u} \tag{67}$$

It is easy to check that the Gaussian data vector $\boldsymbol{z}$ in (65) is uncorrelated with the mean $(\sqrt{E_s}/\alpha)\boldsymbol{v}$ and covariance matrix equal to $[N_0/2]\boldsymbol{I}_K$, where $\boldsymbol{I}_K$ is the $K \times K$ identity matrix. It turns out that for large values of K, $\|\boldsymbol{v}\|^2$ has a closed-form approximation given by Proposition 6 below. This will be used to express the CLRB in a compact expression.

Proposition 6:

$$\|\boldsymbol{v}\|^2 \underset{K\to\infty}{\to} \left[\frac{2\mu_0^2\alpha\varepsilon}{\mu_0 + \alpha\varepsilon}\right] K \tag{68}$$

Proof of Proposition 6: Using (67),

$$\|\boldsymbol{v}\|^2 = \boldsymbol{v}^{*T}\boldsymbol{v} = \mu_0^2\, \boldsymbol{u}^T(\boldsymbol{L}\boldsymbol{L}^T)^{-1}\boldsymbol{u}. \tag{69}$$

from (63) and (64), $\boldsymbol{u}$ is an eigenvector of $\boldsymbol{L}\boldsymbol{L}^T$ with eigenvalue $\hat{\mathcal{S}}_1$, that is,

$$\boldsymbol{L}\boldsymbol{L}^T\boldsymbol{u} = \hat{\mathcal{S}}_1\boldsymbol{u} \tag{70}$$

where $\hat{\mathcal{S}}_1$ is given by

$$\hat{\mathcal{S}}_1 = \sum_{n=0}^{K-1} \hat{p}\,(n\alpha\varepsilon T). \tag{71}$$

Using (24), along with the symmetry of $\hat{p}(.)$, and the fact that $\hat{p}\,(0) = 1$, we obtain

$$\lim_{K\to\infty} \hat{\mathcal{S}}_1 = \frac{1}{2}\left[\frac{\mu_0}{\varepsilon\alpha} + 1\right] \tag{72}$$

hence,

$$\begin{aligned} K &= \boldsymbol{u}^T\boldsymbol{u} = \boldsymbol{u}^T\left(\boldsymbol{L}\boldsymbol{L}^T\right)^{-1}\left(\boldsymbol{L}\boldsymbol{L}^T\right)\boldsymbol{u} \\ &= \hat{\mathcal{S}}_1\boldsymbol{u}^T\left(\boldsymbol{L}\boldsymbol{L}^T\right)^{-1}\boldsymbol{u} \\ &= \frac{\hat{\mathcal{S}}_1\|\boldsymbol{v}\|^2}{\mu_0^2} \end{aligned} \tag{73}$$

$$\Leftrightarrow \|\boldsymbol{v}\|^2 = \frac{\mu_0^2 K}{\hat{\mathcal{S}}_1} \tag{74}$$

(72) and (74) lead to the result of (68), thus completing the proof of Proposition 6. To simplify the derivations of the CRLB, let $\boldsymbol{\theta}$ denote the vector parameter to be estimated as:

$$\boldsymbol{\theta} = [\theta_1 \quad \theta_2 \quad \theta_3] = \left[\sqrt{E_s} \quad \frac{N_0}{2} \quad \frac{1}{\alpha}\right]. \tag{75}$$

Hence, the natural logarithm of the pdf of the complex random vector $\boldsymbol{z}$ in (65) is given by:

$$\begin{aligned} \ln\left(p\left(\boldsymbol{z},\boldsymbol{\theta}\right)\right) = &-Kln\left(2\pi\right) - Kln\left(\theta_2\right) \\ &- \frac{1}{2\theta_2}\sum_k |z_k - \theta_1\theta_3 v_k|^2 \end{aligned} \tag{76}$$

Let $\boldsymbol{g}(\boldsymbol{\theta})$ be the function of the parameter $\boldsymbol{\theta}$ to yield the SNR in dB and SPR on a linear scale. Hence,

$$\boldsymbol{g}\left(\boldsymbol{\theta}\right) = \left[g_1\left(\boldsymbol{\theta}\right) \quad g_2\left(\boldsymbol{\theta}\right)\right] = \left[10\log\left(\frac{\theta_1^2}{2\theta_2}\right) \quad \frac{1}{\theta_3}\right] \tag{77}$$

The CRLBs for the joint SNR and SPR estimation are given by [30]

$$CRLB_i = \left(\left[\frac{\partial \boldsymbol{g}\left(\boldsymbol{\theta}\right)}{\partial\boldsymbol{\theta}}\right] \quad \boldsymbol{I}^{-1}\left[\frac{\partial \boldsymbol{g}\left(\boldsymbol{\theta}\right)}{\partial\boldsymbol{\theta}}\right]^T\right)_{ii} \tag{78}$$

where $i = 1$ for the SNR and $i = 2$ for the SPR, with $(\boldsymbol{A})_{ij}$ denoting the ij^{th}entry of a given matrix $\boldsymbol{A}$, and $\boldsymbol{I}$ is the Fisher information matrix (FIM) [30] defined by

$$I_{ij} = -E\left\{\frac{\partial^2\ln\left(p\left(\boldsymbol{z},\boldsymbol{\theta}\right)\right)}{\partial\theta_i\partial\theta_j}\right\} \tag{79}$$

From (76)-(79), we get

$$\frac{\partial \boldsymbol{g}\left(\boldsymbol{\theta}\right)}{\partial\boldsymbol{\theta}} = \begin{bmatrix} \dfrac{20}{\ln\left(10\right)\theta_1} & \dfrac{-10}{\ln\left(10\right)\theta_2} & 0 \\ 0 & 0 & \dfrac{-1}{\theta_3^2} \end{bmatrix} \tag{80}$$

$$I_{11} = \frac{\theta_3^2\|\boldsymbol{v}\|^2}{\theta_2} \tag{81}$$

$$I_{22} = \frac{K}{\theta_2^2} \tag{82}$$

$$I_{33} = \frac{\theta_1^2\|\boldsymbol{v}\|^2}{\theta_2} \tag{83}$$

$$I_{31} = I_{13} = \frac{\theta_1\theta_3\|\boldsymbol{v}\|^2}{\theta_2} \tag{84}$$

$$I_{21} = I_{12} = I_{23} = I_{32} = 0 \tag{85}$$

It turns out that matrix I is singular; hence, the generalized Moore-Penrose inverse [31], denoted by $I^{\dagger}$ is used instead of I^{-1} in (78) and is found to be

$$I^{\dagger} = a\begin{bmatrix} 1 & 0 & b \\ 0 & c & 0 \\ b & 0 & b^2 \end{bmatrix} \tag{86}$$

where

$$a = \frac{\theta_2\theta_3^2}{\|\boldsymbol{v}\|^2(\theta_3^2 + \theta_1^2)} \tag{87}$$

$$b = \frac{\theta_1}{\theta_3} \tag{88}$$

$$c = \frac{\theta_2^2}{aK} \tag{89}$$

Using (86)-(89) in (78), and after some simplifications, we obtain, using (68), the joint FTN CRLB for the SNR and SPR (for a large K) as

$$\begin{aligned} CRLB_{J\_FTN\_SNR} &= \frac{100}{\ln^2\left(10\right)}\left[\frac{1}{K} + \frac{2\alpha^2}{SNR\|\boldsymbol{v}\|^2(1+\alpha^2E_s)^2}\right] \\ &\approx \frac{100}{\ln^2\left(10\right)K}\left[1 + \frac{\alpha(\mu_0+\alpha\varepsilon)}{\mu_0^2\varepsilon(SNR)(1+\alpha^2E_s)^2}\right] \end{aligned} \tag{90}$$

$$\begin{aligned} CRLB_{J\_FTN\_\alpha} &= \frac{\alpha^4}{2SNR\|\boldsymbol{v}\|^2(1+\frac{1}{\alpha^2E_s})^2} \\ &\approx \frac{\alpha^3(\mu_0+\alpha\varepsilon)}{4K\mu_0^2\varepsilon(SNR)(1+\frac{1}{\alpha^2E_s})^2} \end{aligned} \tag{91}$$

where the SNR unit in (90) and (91) is on a linear scale, while $CRLB_{J\_FTN\_SNR}$ is in dB^2. The singularity of the FIM [31] makes the joint CRLBs in (89) and (90) rather optimistic (loose). Tighter CLRBs may be obtained in the context of individually estimating the SNR and SPR. Assuming α to be known, the single CLRB for the SNR follows by using the upper-left 2-by-2 block of the FIM above in (81)-(85) as well as the upper 1-by-2 vector of $\partial \boldsymbol{g}(\boldsymbol{\theta})/\partial \boldsymbol{\theta}$ in (80). After some simplifications, using (68), we obtain for a large K

$$\begin{aligned} CRLB_{s\_FTN\_SNR} &= \frac{100}{\ln^2(10)}\left[\frac{1}{K}+\frac{2\alpha^2}{SNR\|\boldsymbol{v}\|^2}\right] \\ &\approx \frac{100}{\ln^2(10)\,K}\left[1+\frac{\alpha(\mu_0+\alpha\varepsilon)}{\mu_0^2\varepsilon\,(SNR)}\right] \end{aligned} \tag{92}$$

Likewise, the single CRLB for the SPR can be obtained after some simplifications as

$$CRLB_{s\_FTN\_\alpha} = \left[\frac{\partial g_2(\theta)}{\partial \theta_3}\right]^2 I_{33}^{-1} \approx \frac{\alpha^3(\mu_0+\alpha\varepsilon)}{4\mu_0^2\varepsilon K(SNR)} \tag{93}$$

It can be seen from (90)-(93) that the joint CRLBs for both SNR and SPR are upper bounded by the single CRLBs. For the sake of simplicity, the tighter single CRLBs for the SNR and SPR in (90) and (91) will be used to benchmark the estimators in the next section and are denoted by $CRLB_{FTN\_SNR}$ and $CRLB_{FTN\_\alpha}$. Note that in the case of Nyquist signaling (i.e., no ISI with $\alpha = 1$, $\beta = 0$, $\varepsilon = 1$ leading to the fact that $\mu_0 = 1$ in the DA FTN signal model of (50) owing to the fact that $\hat{p}(0) = 1$ and $\hat{p}(nT) = 0$ for $n \neq 0$), the matrix $\boldsymbol{C}_{\hat{w}}$ in (64) is diagonal and $\boldsymbol{L}$ is the K *by* K identity matrix. Hence, $\|\boldsymbol{v}\|^2 = K$ and the $CRLB_{FTN\_SNR}$ in (90) tends for a large sample size K to the standard DA-CRLB [21] given by

$$CRLB_{Nyq\_SNR} = \frac{100}{\ln^2(10)\,K}\left[1+\frac{2}{SNR}\right] \tag{94}$$

VI. COMPUTER SIMULATIONS FOR THE SPECIAL CASE OF THE RRC PULSE

In this section, we present the results of the computer simulations that we carried out to illustrate the theoretical derivations and the performance of the proposed estimators for the special case of the commonly used RRC signaling pulse. The simulations targeted the effect the following parameters on the MSE performance of the estimators:

- SNR
- SPR
- The sampling phase error (β)
- The sampling frequency errors (ε)
- The sample size K
- The pulse roll-off factor (r)
- The modulation type and level

Because the carrier phase term ϕ is irrelevant in the calculation of all the even-ordered moments (including the magnitude of the first moment for the DA estimators), it is set to zero throughout all the computer simulations. All moments were estimated using time-averages, namely, $\mathcal{M}_{y_{2q}}$ is calculated by

$$\tilde{\mathcal{M}}_{y_{2q}} = \frac{1}{K}\sum_{n=0}^{K}(y[n])^q\left(y^*[n]\right)^q. \tag{95}$$

In addition, all estimator variances were estimated over 500 trials. We subjectively judged a 24-sample ISI (12 samples before and after the sample of interest) to provide a good compromise between accuracy and simulation time, as we experimentally observed that increasing the ISI extent to larger values would greatly prolong the simulation times but with a negligible effect on the results. The same window extent was also used to find $\hat{w}(t)$ while convolving the AWGN $w(t)$ with the RRC pulse $p(t)$ defined by

$$p(t) = \begin{cases} 1+r(-1+4/\pi) & \textit{for } t=0 \\ \dfrac{r}{\sqrt{2}}\left[\sin\left(\dfrac{\pi}{4r}\right)\left(1+\dfrac{2}{\pi}\right)+\cos\left(\dfrac{\pi}{4r}\right)\left(1-\dfrac{2}{\pi}\right)\right], & \\ \qquad \textit{for } |t| = \dfrac{T}{4r} & \\ \dfrac{\left[\sin\left(\frac{\pi t(1-r)}{T}\right)+\frac{4rt}{T}\cos\left(\frac{\pi t(1+r)}{T}\right)\right]}{\frac{\pi t}{T}\left[1-(4rt/T)^2\right]} & \end{cases} \tag{96}$$

with its squared magnitude spectrum

$$\begin{aligned} \hat{P}_0(f) &\equiv |P(f)|^2 \\ &= \begin{cases} T; & \textit{for } |f| \le (1-r)/(2T) \\ \dfrac{T}{2}\left[1+\cos\left(\dfrac{T\pi}{r}\left(|f|-\dfrac{(1-r)}{2T}\right)\right)\right], & \\ \qquad \textit{for } \dfrac{1}{2T}(1-r) \le |f| \le \dfrac{1}{2T}(1+r) & \end{cases} \end{aligned} \tag{97}$$

and auto-correlation

$$\hat{p}(t) = \left[\frac{sinc(t/T)\cos(\pi rt/T)}{1-(2rt/T)^2}\right], \tag{98}$$

where r in (96)-(98) above denotes the roll-off factor. For this special case, the support of $P(f)$ is reduced from $1/T$ to $(1+r)/2T$ leading to the fact that $\hat{P}_{k-1}(f) = 0$ for $|f| > k(1+r)/2T$ (k $= 1, 2, \ldots$). As a result, the tighter sufficient condition related to $\mathcal{S}_k$ in (24) is relaxed to $0 < \alpha \le 2/[k(1+r)]$. As illustrated in the next section, computer simulations indicate that it is practically possible to further relax this range without a considerable loss of accuracy in the estimation results. Referring to (5), (25), and (97), we obtain:

$$\mu_0 = \frac{|P(0)|^2}{T} = 1 \tag{99}$$

for $0 < \alpha \le 1$ and $0 \le r \le 1$, and

$$\mu_1 = \frac{\hat{P}_1(0)}{T} = 2\int_0^{1/T}|P(f)|^4\,df = 1-\frac{r}{4}; \tag{100}$$

with the sufficient condition $0 < \alpha \le 1/(1+r)$ and $0 \le r \le 1$. The evaluation of $\mu_3$and μ_5 from (5) requires

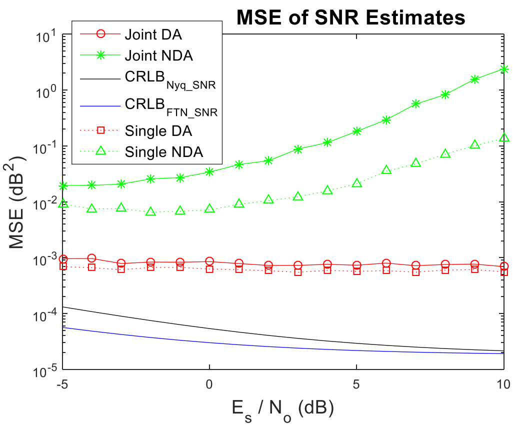

FIGURE 1. SNR Estimator MSE versus SNR for QPSK with $r = 0.1$, $\alpha = 0.45$, $\beta = 0.15$, $\varepsilon = 0.95$, and $K = 10^6$.

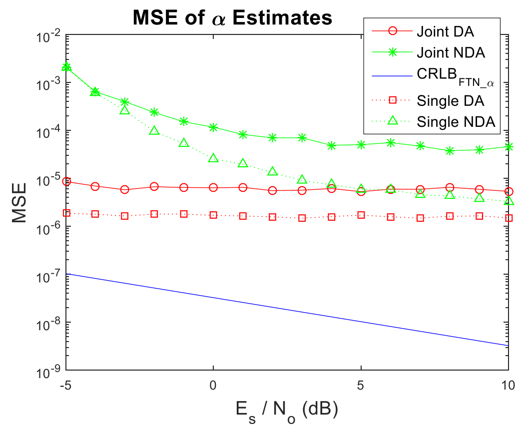

FIGURE 2. SPR Estimator MSE versus SNR for QPSK with $r = 0.1$, $\alpha = 0.45$, $\beta = 0.15$, $\varepsilon = 0.95$, and $K = 10^6$.

finding $\hat{P}_1(f)$ and $\hat{P}_2(f)$, respectively, the first- and second-order auto-convolution of $\hat{P}_0(f)$. Lengthy but straightforward integrations that we carried out with the help of symbolic computer calculations led to

$$\mu_3 = \frac{2}{3} + \left(\frac{8}{\pi^2} - 1\right) r^2 + \left(\frac{25}{32} - \frac{453}{64\pi^2}\right) r^3 \quad (101)$$

with the *sufficient* condition $0 < \alpha \leq 1/2(1+r)$ and $0 \leq r \leq 1/2$.

$$\mu_5 = \frac{11}{20} + \left(\frac{6}{\pi^2} - \frac{3}{4}\right) r^2 + \frac{3}{2\pi^4}\left(84 - 18\pi^2 + \pi^4\right) r^4 - \frac{1}{2048\pi^4}\left(348705 - 58485\pi^2 + 2389\pi^4\right) r^5 \quad (102)$$

with the *sufficient* condition $0 < \alpha \leq 1/3(1+r)$ and $0 \leq r \leq 1/3$.

A. ESTIMATOR MSE VARIATIONS WITH RESPECT TO SNR

Fig. 1 depicts the variations of the SNR estimators with respect to the SNR ($= E_s/N_0$) of the FTN signal for QPSK modulation with $r = 0.1$, $\alpha = 0.45$, $\beta = 0.1$, $\varepsilon = 0.95$, and $K = 10^6$. It is seen that the joint NDA estimator is, on average, one order of magnitude less efficient than its NDA single counterpart, with a more pronounced gap for higher SNR. Generally, the MSE for both estimators exhibits an upward slope as the SNR increases. On the other hand, the DA estimators seem invariant to the SNR with a noticeably smaller gap in MSE between the joint and single estimators. Both DA estimators have an MSE that is between one and two orders of magnitude smaller than their NDA counterparts, and one order of magnitude higher than the $CRLB_{FTN\_SNR}$.

Fig. 2 is analogous to Fig. 1 in that it depicts the variations of the SPR estimators with respect to the SNR of the FTN signal for QPSK modulation with $r = 0.1$, $\alpha = 0.45$, $\beta = 0.1$, $\varepsilon = 0.95$, and $K = 10^6$. It shows that the joint NDA estimator produces an MSE that is comparable to that of the single NDA estimator for lower SNR values

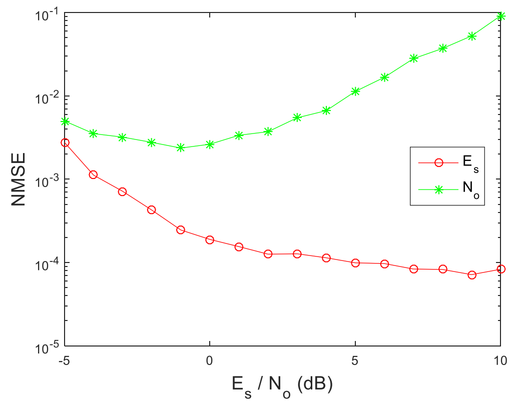

FIGURE 3. Joint (E_s, N_o) NDA Estimator NMSE versus SNR for QPSK with $r = 0.1$, $\alpha = 0.45$, $\beta = 0.15$, $\varepsilon = 0.95$, and $K = 10^6$.

(close to -5 dB), increasing to approximately one order of magnitude for a higher SNR (close to 10 dB). The MSE for both estimators exhibits a downwards slope as the SNR increases. The DA estimators seem invariant to the SNR with a gap in MSE of approximately half an order of magnitude between the joint and single estimators. The DA estimators have an MSE that is between two and three orders of magnitude smaller than their NDA counterparts for a smaller SNR (less than zero), decreasing to approximately one order of magnitude for a higher SNR (close to 10 dB). In addition, the variance of the DA SPR estimators is one to two orders of magnitude higher than that of $CRLB_{FTN\_\alpha}$ for smaller SNR values increasing to three orders of magnitude for higher SNR values.

Finally, Fig. 3 illustrates the normalized MSE (NMSE) of the explicit joint NDA estimators of E_s and N_o versus SNR for QPSK modulation with $r = 0.1$, $\alpha = 0.45$, $\beta = 0.1$, $\varepsilon = 0.95$, and $K = 10^6$. This indicates that while the NDA estimator variance for both E_s (and α, as shown in Fig. 2) decreases with increasing SNR, this dependency is reversed for N_0 in agreement with the upward slope of the NDA estimators in Fig. 1.

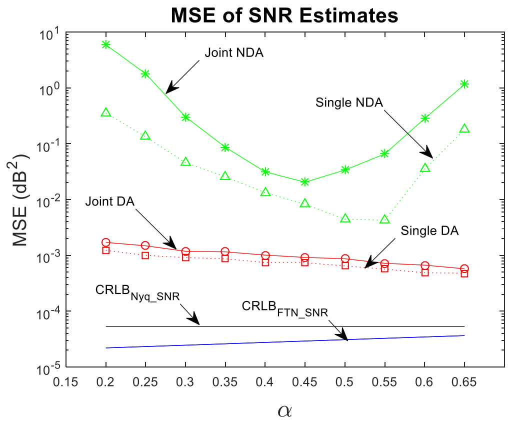

FIGURE 4. SNR Estimator MSE versus SPR for QPSK with $r = 0.1$, $\beta = 0.15$, $\varepsilon = 0.95$, SNR $= 0$ dB, and $K = 10^6$.

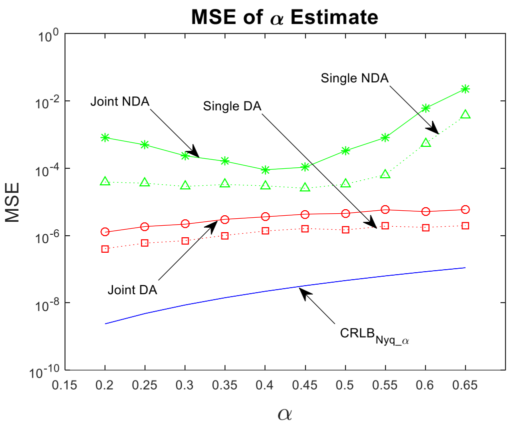

FIGURE 5. SPR Estimator MSE versus SPR for QPSK with $r = 0.1$, $\beta = 0.15$, $\varepsilon = 0.95$, SNR $= 0$ dB, and $K = 10^6$.

B. ESTIMATOR MSE VARIATIONS WITH RESPECT TO SPR

Fig. 4 shows the variations of the SNR estimators with respect to SPR for QPSK modulation with $r = 0.1$; $\beta = 0.15$; $\varepsilon = 0.95$; SNR $= 0$ dB, $K = 10^6$. The joint NDA estimator is approximately one order of magnitude less efficient than its NDA single counterpart for smaller and higher values of α. This gap is approximately halved for α around 0.45 where the MSE for both NDA estimators exhibited a minimum. The degradation in MSE above this value is attributed to exceeding the conditions in (100)-(102). On the other hand, the DA estimators exhibit less variation in MSE with respect to $\boldsymbol{\alpha}$ with a light downward slope. Both DA estimators have an MSE that is approximately one order of magnitude higher than the $CRLB_{FTN\_SNR}$.

Fig. 5 depicts the MSE of the SPR estimators versus α for QPSK modulation with $r = 0.1$; $\beta = 0.15$; $\varepsilon = 0.95$; SNR $=$ 0 dB, $K = 10^6$. The results are similar to those in Fig. 4, with a moderately larger gap in MSE between the DA joint and single estimators.

C. ESTIMATOR MSE VARIATIONS WITH RESPECT TO SAMPLING PHASE ERRORS (β)

Fig. 6 and 7 illustrate the variations of the estimators' MSE (SNR and SPR, respectively) with respect to the sampling phase errors ($|\beta|$) for QPSK modulation with $r = 0.1$, $\alpha =$ 0.45, $\varepsilon = 0.95$, SNR $= 0$ dB, and $K = 10^6$. It can be seen from both figures that, aside from the expected variations due to averaging over a finite trial size, the MSEs of all the estimators are independent of $|\beta|$, reflecting one of the aspects of the robustness of the proposed estimators.

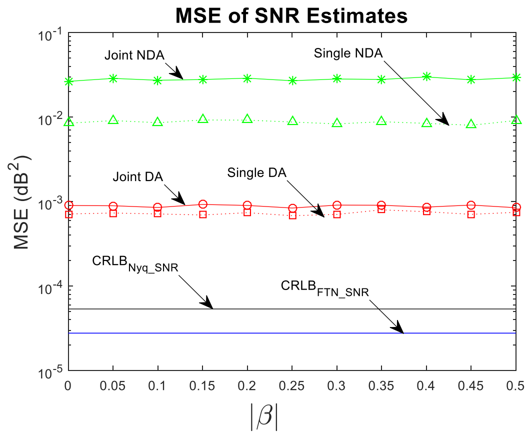

FIGURE 6. SNR Estimator MSE versus $|\beta|$ for QPSK with $r = 0.1$, $\alpha = 0.45$, $\varepsilon = 0.95$, SNR $= 0$ dB, and $K = 10^6$.

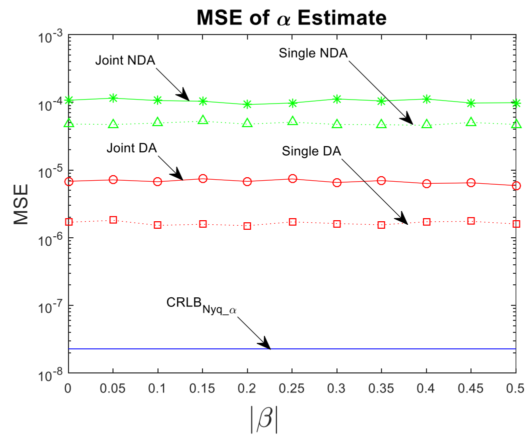

FIGURE 7. SPR Estimator MSE versus $|\beta|$ for QPSK with $r = 0.1$, $\alpha = 0.45$, $\varepsilon = 0.95$, SNR $= 0$ dB, and $K = 10^6$.

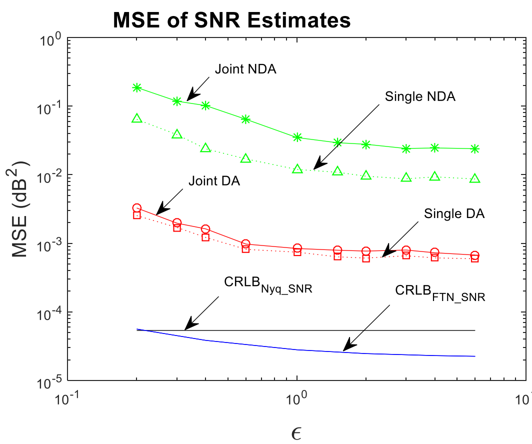

FIGURE 8. SNR Estimator MSE versus ε for QPSK with $r = 0.1$, $\alpha = 0.45$, $\beta = 0.15$, SNR $= 0$ dB, and $K = 10^6$.

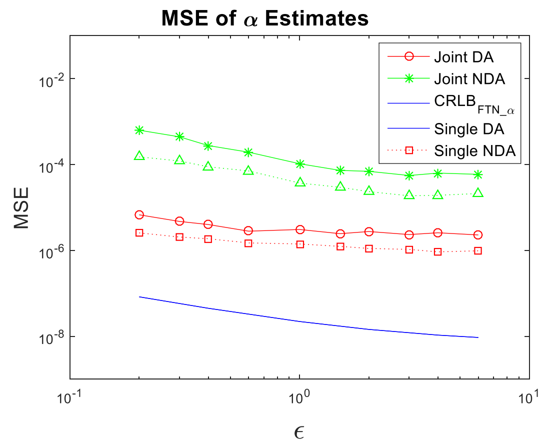

FIGURE 9. SPR Estimator MSE versus ε for QPSK with $r = 0.1$, $\alpha = 0.45$, $\beta = 0.15$, SNR = 0 dB, and $K = 10^6$.

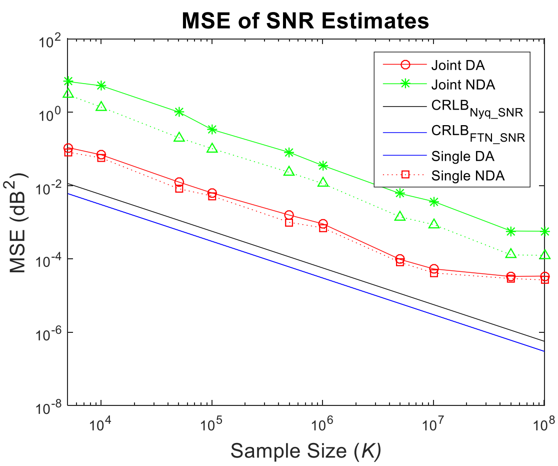

FIGURE 10. SNR Estimator MSE versus K for QPSK with $r = 0.1$, $\alpha = 0.45$, $\beta = 0.15$, SNR = 0 dB, and $\varepsilon = 0.95$.

D. ESTIMATOR MSE VARIATIONS WITH RESPECT TO SAMPLING FREQUENCY ERRORS (ε)

Fig. 8 and 9 illustrate the variations of the estimators' MSE (SNR and SPR, respectively) with respect to the sampling frequency errors (= ε) for QPSK modulation with r = 0.1, $\alpha = 0.45$, $\beta = 0.15$, SNR = 0 dB, and K = 10^6. It can be seen from figure 9 that the MSE for the SPR estimators exhibits little variation for $\varepsilon \geq 0.5$ and slightly increases with a smaller ε below 0.5. Fig. 8 depicts a similar MSE profile for the SNR estimators, except that it increases with a slightly higher slope for a smaller ε below 0.5. Both figures indicate that it is plausible to assume that the performance of the proposed estimators remains fairly invariant to sampling frequency errors corresponding to $\varepsilon \geq 0.5$, a range that is expected to be practical, especially with some a priori knowledge about the SPR.

E. ESTIMATOR MSE VARIATIONS WITH RESPECT TO SAMPLE SIZE (K)

Fig. 10 and 11 illustrate the variations of the estimators' MSE (SNR and SPR, respectively) with respect to the sample size

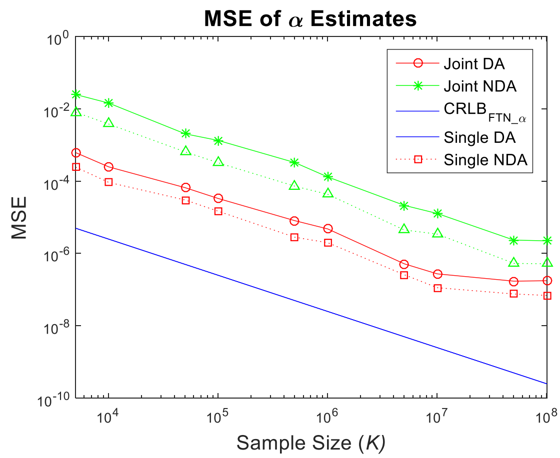

FIGURE 11. SPR Estimator MSE versus K for QPSK with $r = 0.1$, $\alpha = 0.45$, $\beta = 0.15$, SNR = 0 dB, and $\varepsilon = 0.95$.

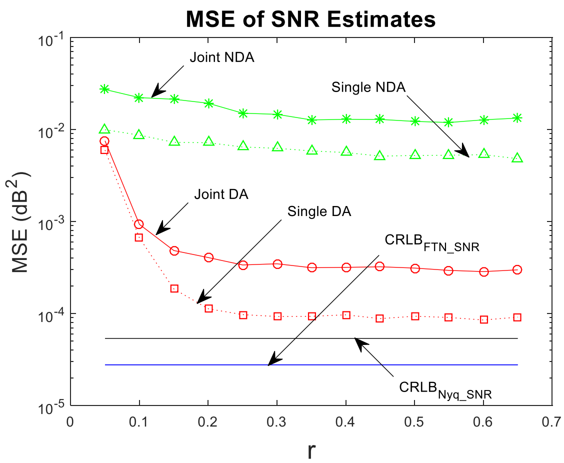

FIGURE 12. SNR Estimator MSE versus r for QPSK with $\alpha = 0.45$, $\beta = 0.15$, SNR = 0 dB, $\varepsilon = 0.95$, and $K = 10^6$.

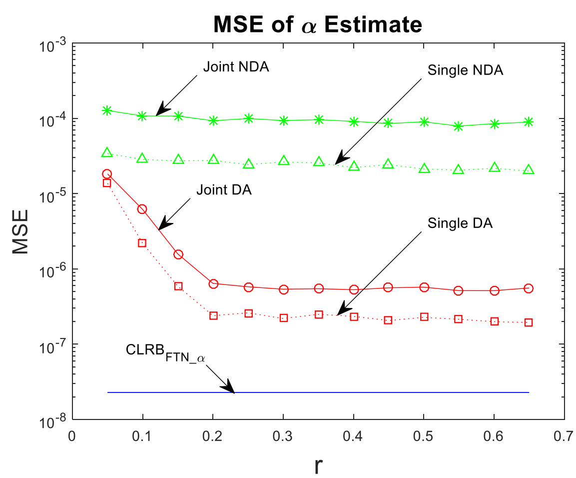

FIGURE 13. SPR Estimator MSE versus r for QPSK with $\alpha = 0.45$, $\beta = 0.15$, SNR = 0 dB, $\varepsilon = 0.95$, and $K = 10^6$.

(K) for QPSK modulation with $r = 0.1$, $\alpha = 0.45$, $\beta = 0.15$, SNR $= 0$ dB, and $\varepsilon = 0.95$. It can be seen from both figures that the MSE monotonically decreases with an increase in K with a flattened profile at and above $K = 5 \times 10^7$.

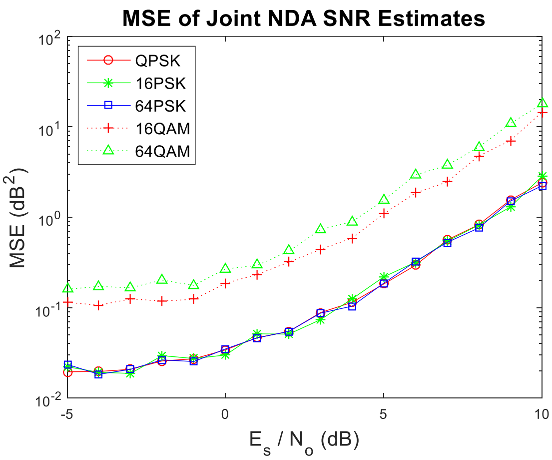

FIGURE 14. Joint NDA SNR Estimator MSE versus SNR for different modulation types and levels with $r = 0.1$, $\alpha = 0.45$, $\beta = 0.15$, $\varepsilon = 0.95$, and $K = 10^6$.

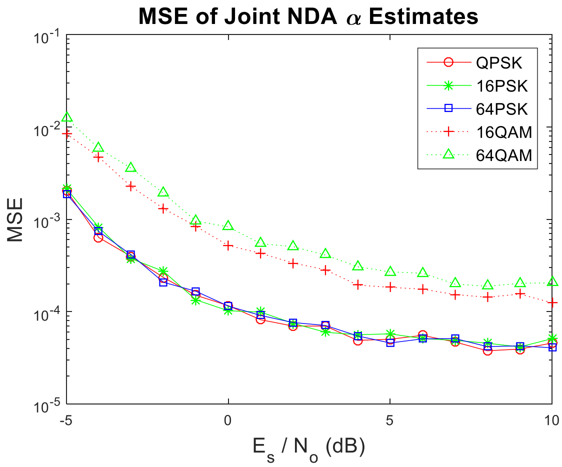

FIGURE 15. Joint NDA SPR Estimator MSE versus SNR for different modulation types and levels with $r = 0.1$, $\alpha = 0.45$, $\beta = 0.15$, $\varepsilon = 0.95$, and $K = 10^6$.

F. ESTIMATOR MSE VARIATIONS WITH RESPECT TO THE ROLL-OFF FACTOR (r)

Fig. 12 and 13 illustrate the variations in the Estimators' MSE (SNR and SPR, respectively) with respect to the RRC pulse roll-off factor ($= r$) for QPSK modulation with $\alpha = 0.45$, $\beta = 0.15$, SNR $= 0$ dB, and $\varepsilon = 0.95$, and $K = 10^6$. For both SNR and SPR, the NDA estimators exhibit little variations with respect to " r", while for DA the performance of the estimators sharply decreases for values of r below 0.2 and remain fairly constant above this value.

G. ESTIMATOR MSE VARIATIONS WITH RESPECT TO THE MODULATION TYPE AND LEVEL

Fig. 14 and 15 illustrate the variations in the Joint NDA Estimators' MSE (SNR and SPR, respectively) with respect to the SNR for M-PSK (M = 4, 16, 64) and M-QAM (M = 16, 64) with $r = 0.1$, $\alpha = 0.45$, $\beta = 0.15$, SNR $= 0$ dB, and $K = 10^6$. Fig. 16 and 17 are analogous to 14 and 15 except for the single NDA estimators. It can be seen from these figures that for both SNR and SPR, the MSE

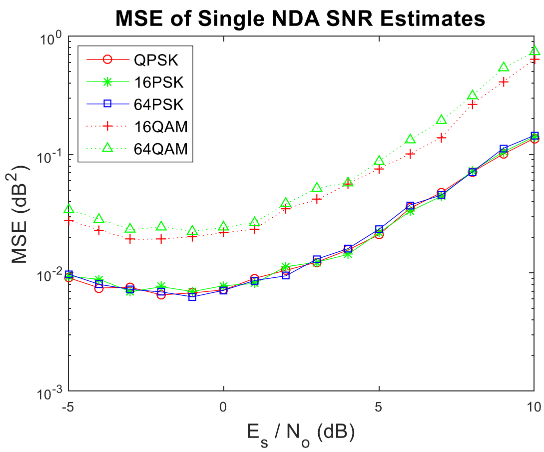

FIGURE 16. Single NDA SNR Estimator MSE versus SNR for different modulation types and levels with $r = 0.1$, $\alpha = 0.45$, $\beta = 0.15$, $\varepsilon = 0.95$, and $K = 10^6$.

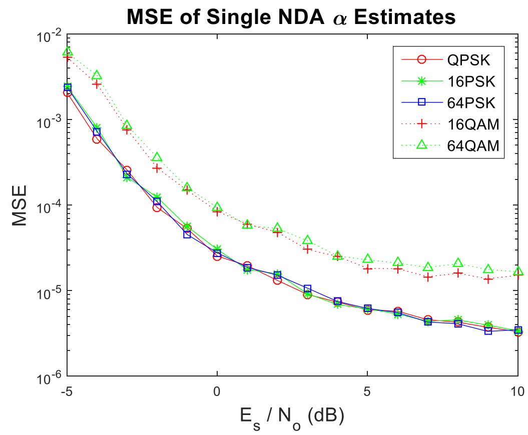

FIGURE 17. Single NDA SPR Estimator MSE versus SNR for different modulation types and levels with $r = 0.1$, $\alpha = 0.45$, $\beta = 0.15$, $\varepsilon = 0.95$, and $K = 10^6$.

of the estimators for the equal-energy signal constellations (M-PSK) are approximately half an order of magnitude more efficient than their non-equal-energy counterparts (M-QAM). The modulation level seemed to slightly effect the latter, with no noticeable impact on the former.

VII. CONCLUSION

In this work, we presented novel, robust, and computationally attractive DA and NDA estimators for the two main parameters of the FTN signal, namely SNR and SPR. The estimators are robust in the sense that they are insensitive to carrier and sampling errors. By including the sixth statistical moment (M6) alongside the fourth (M4) and second (M2), it is possible to provide, for the first time, a joint blind estimator for both parameters. Single NDA estimators were also provided using up to M4 only and turn out to be approximately one order of magnitude more efficient than their joint counterparts. DA estimators were also proposed that use up to M2 only and provide two to three orders of magnitude reduction in MSE compared to their blind counterparts. To benchmark the estimator's efficiency, novel and compact DA CRLBs were derived, for SPR and SNR. In the limiting case of Nyquist signaling, the FTN SNR CRLB was shown to be identical to the standard DA CRLB. The RRC signaling pulse was used as a special case of the general estimator derivations, providing some of the required estimator parameters in compact closed-form expressions in terms of the pulse roll-off factor r. Extensive computer simulations were applied to this special case to validate the derivations and illustrate the MSE performance of the proposed estimators. They were found to work best for the practical range of low SNR values (close to 0 dB) and moderate SPR values (close to 0.4).

Despite the relatively low efficiencies (with reference to the CRLBs) of the proposed estimators, their computational features in addition to their robustness against carrier and sampling errors, make them valuable in many practical applications that incorporate cognitive radio alongside FTN.

REFERENCES

[1] J. E. Mazo, "Faster-than-Nyquist signaling," *Bell Syst. Tech. J.*, vol. 54, no. 8, pp. 1451–1462, 1975.

[2] J. B. Anderson, F. Rusek, and V. Öwall, "Faster-than-Nyquist signaling," *Proc. IEEE*, vol. 101, no. 8, pp. 1817–1830, Aug. 2013.

[3] M. Jana, L. Lampe, J. Mitra, W. Jin, and K. Law, "Probabilistic shaping in time-frequency-packed Terabit superchannel transmission," *IEEE Photon. Technol. Lett.*, vol. 32, no. 17, pp. 1065–1068, Sep. 1, 2020.

[4] Y. Zhu, M. Jiang, Z. Chen, and F. Zhang, "Terabit faster-than-Nyquist PDM 16-QAM WDM transmission with a net spectral efficiency of 7.96 b/s/Hz," *J. Lightw. Technol.*, vol. 36, no. 14, pp. 2912–2919, Jul. 15, 2018.

[5] Q. Li, Y. Gao, F.-K. Gong, W.-Y. Zhao, H.-Y. Ding, and Y. Zhang, "PAPR analysis for faster-than-Nyquist signaling in satellite communications," in *Proc. Int. Conf. Wireless Commun. Signal Process. (WCSP)*, Oct. 2020, pp. 708–711.

[6] A. Piemontese, A. Modenini, G. Colavolpe, and N. S. Alagha, "Improving the spectral efficiency of nonlinear satellite systems through time-frequency packing and advanced receiver processing," *IEEE Trans. Commun.*, vol. 61, no. 8, pp. 3404–3412, Aug. 2013.

[7] Q. Li, F.-K. Gong, P.-Y. Song, G. Li, and S.-H. Zhai, "Beyond DVB-S2X: Faster-than-Nyquist signaling with linear precoding," *IEEE Trans. Broadcast.*, vol. 66, no. 3, pp. 620–629, Sep. 2020.

[8] S. Liu, Y. Qiao, X. Tang, M. Guo, X. Xu, Z. Sun, H. Cui, and Y. Lu, "Simplified soft-output direct detection FTN algorithm for 56-Gb/S optical PAM-4 system using 10G-class optics," *IEEE Access*, vol. 8, pp. 104518–104526, 2020.

[9] Y. Shao, Y. Hong, S. Gao, and L.-K. Chen, "Faster-than-Nyquist DFT-S-OFDM over visible light communications," in *Proc. 23rd Opto-Electron. Commun. Conf. (OECC)*, Jul. 2018, pp. 1–2.

[10] J. C. P. Garcia, E. O. Guerra, C. H. Barriquello, M. A. D. Costa, and V. A. Reguera, "Faster-than-Nyquist signaling for physical layer security on wireless smart grid," in *Proc. IEEE PES Innov. Smart Grid Technol. Conf.-Latin Amer. (ISGT Latin Amer.)*, Sep. 2019, pp. 1–6.

[11] K. Wang, Y. Lu, L. Liu, B. Mao, B. Wu, Y. Huang, R. Mo, Y. Wang, and L. Li, "Dual-carrier 400G field trial submarine transmission over 6,577-km using 60-GBaud digital faster-than-Nyquist shaping PDM-QPSK modulation format," in *Proc. Opt. Fiber Commun. Conf.*, 2015, pp. 1–3.

[12] B. G. Jo, M. C. Park, and D. S. Han, "SM-MIMO scheme with FTN signalling for UHDTV," in *Proc. IEEE Int. Conf. Consum. Electron. (ICCE)*, Jan. 2016, pp. 514–515.

[13] J. Anderson, *Faster-Than-Nyquist Signaling for 5G Communication*. Hoboken, NJ, USA: Wiley, 2016, pp. 24–46.

[14] B. Lee, J. Kim, H. Lee, B. Shim, Y. Kim, and J. Lee, "Towards faster-than-Nyquist transmission for beyond 5G wireless communications," in *Proc. IEEE Int. Conf. Commun. (ICC)*, May 2019, pp. 1–6.

[15] A. Prjla and J. Anserson, "Reduced-complexity receivers for strongly narrowband intersymbol interference introduced by faster-than-Nyquist signaling," *IEEE Trans. Commun.*, vol. 60, no. 9, pp. 2591–2601, Sep. 2012.

[16] I. Kakalou, K. E. Psannis, P. Krawiec, and R. Badea, "Cognitive radio network and network service chaining toward 5G: Challenges and requirements," *IEEE Commun. Mag.*, vol. 55, no. 11, pp. 145–151, Nov. 2017.

[17] D. R. Pauluzzi and N. C. Beaulieu, "A comparison of SNR estimation techniques for the AWGN channel," *IEEE Trans. Commun.*, vol. 48, no. 10, pp. 1681–1691, Oct. 2000.

[18] R. Matzner and F. Englberger, "An SNR estimation algorithm using fourth-order moments," in *Proc. IEEE Int. Symp. Inf. Theory*, Jun./Jul. 1994, p. 119.

[19] R. Lopez-Valcarce and C. Mosquera, "Sixth-order statistics-based non-data-aided SNR estimation," *IEEE Commun. Lett.*, vol. 11, no. 4, pp. 351–353, Apr. 2007.

[20] X. Liang, A. Liu, X. Pan, and G. Wu, "EM-based SNR estimator for faster-than-Nyquist signalling system," *Electron. Lett.*, vol. 51, no. 24, pp. 2051–2053, Nov. 2015.

[21] N. S. Alagha, "Cramer–Rao bounds of SNR estimates for BPSK and QPSK modulated signals," *IEEE Commun. Lett.*, vol. 5, no. 1, pp. 10–12, Jan. 2001.

[22] A. Napolitano, "Cyclostationarity: New trends and applications," *Signal Process.*, vol. 120, pp. 385–408, Mar. 2016.

[23] P. Song, F. Gong, and Q. Li, "Blind symbol packing ratio estimation for faster-than-Nyquist signalling based on deep learning," *Electron. Lett.*, vol. 55, no. 21, pp. 1155–1157, Oct. 2019.

[24] A. Abello, D. Roque, and J. Freixe, "Blind symbol rate estimation of faster-than-Nyquist signals based on higher-order statistics," in *Proc. IEEE Int. Conf. Cogn. Radio-Oriented Wireless Netw. (CROWNCOM)*, Sep. 2017, pp. 200–210.

[25] A. Barbieri, D. Fertonani, and G. Colavolpe, "Time-frequency packing for linear modulations: Spectral efficiency and practical detection schemes," *IEEE Trans. Commun.*, vol. 57, no. 10, pp. 2951–2959, Oct. 2009.

[26] F. Rusek and J. B. Anderson, "Multi-stream faster-than-Nyquist signaling," *IEEE Trans. Commun.*, vol. 57, no. 5, pp. 1329–1340, May 2009.

[27] H. Cramer, *Mathematical Methods of Statistics*. Princeton, NJ, USA: Princeton Univ. Press, 1957.

[28] T. Adali, P. J. Schreier, and L. L. Scharf, "Complex-valued signal processing: The proper way to deal with impropriety," *IEEE Trans. Signal Process.*, vol. 59, no. 11, pp. 5101–5125, Nov. 2011.

[29] Z. Bahri, "Analytic investigation into the statistical characteristics of the interference due to non-orthogonal time–frequency signaling," *Eng. Sci. Technol., Int. J.*, vol. 20, no. 5, pp. 1430–1438, Oct. 2017.

[30] S. M. Kay, *Fundamentals of Statistical Signal Processing, Estimation Theory*. Englewood Cliffs, NJ, USA: Prentice-Hall, 1993.

[31] P. Stoica and T. L. Marzetta, "Parameter estimation problems with singular information matrices," *IEEE Trans. Signal Process.*, vol. 49, no. 1, pp. 87–90, Jan. 2001.

ZOUHIR BAHRI (Member, IEEE) received the B.Sc. degree in electrical engineering from the University of Pittsburgh, in 1985, and the M.Sc. and Ph.D. degrees *(summa cum laude)* in electrical and computer engineering from Carnegie Mellon University (CMU), in 1986 and 1989, respectively.

Since 1989, he has been with the Department of Electrical and Electronics Engineering, University of Bahrain, which he has pioneered and currently chairing. His current research interests include signal processing for communication and biomedical engineering.

Dr. Bahri is the Co-Founder and an Acting Advisor of the IEEE ComSoc Student Chapter of UOB. He is a reviewer of several international journals. He has been with the technical and organizational committees of several local and international conferences, the latest of which are the Fourth Smart City Symposium (SCS21) and the Second IEEE Middle East and North Africa Communications Conference.